Magnetic Studies on μ-Azido Polynuclear Nickel(II) Compounds with the 222-tet Ligand. Crystal Structure of $(\mu\text{-}N_3)_2[Ni(222\text{-tet})]_2(BPh_4)_2$ (222-tet = Triethylenetetramine) and EXAFS Structural Characterization of the Triangular Compounds $(\mu\text{-}N_3)_3[Ni(222\text{-tet})]_3(X)_3$ ($X = PF_6^-$, ClO_4^-)

Albert Escuer,[†] Isabel Castro,[‡] Franz Mautner,[§] Mohamed Salah El Fallah,[†] and Ramon Vicente*,[†]

Departament de Química Inorgànica, Universitat de Barcelona, Diagonal 647, Barcelona 08028, Spain, Departament de Química Inorgànica, Facultat de Química, Universitat de València, Dr. Moliner 50, 46100 Burjassot, València, Spain, and Institut für Physikalische und Theoretische Chemie, Technische Universität Graz, A-8010 Graz, Austria

Received March 3, 1997[⊗]

The nickel(II) dinuclear 1,3-azido-bridged compound $(\mu\text{-}N_3)_2[Ni(222\text{-tet})]_2(BPh_4)_2$ (**1**) and the trinuclear compounds $(\mu\text{-}N_3)_3[Ni_3(222\text{-tet})_3](PF_6)_3$ (**2**) and $(\mu\text{-}N_3)_3[Ni_3(222\text{-tet})_3](ClO_4)_3$ (**3**) were synthesized and characterized. 222-tet is the tetraaminate ligand triethylenetetramine. The crystal structure of **1** was solved by X-ray diffraction. **1** crystallizes in the monoclinic system: space group $P2_1/n$, $a = 10.639(4)$ Å, $b = 19.770(7)$ Å, $c = 13.609(6)$ Å, $\beta = 97.78(3)°$, $Z = 2$, formula $C_{60}H_{76}B_2N_{14}Ni_2$. In the absence of single crystals of **2** and **3**, we carried out an EXAFS study of **1**−**3** at the nickel K-edge, using compound **1** as a model, in order to obtain structural information for compounds **2** and **3**. The analysis of XANES and EXAFS spectra of compounds **1**−**3** reveals the occurrence of azido-bridged trinuclear nickel(II) compounds for **2** and **3** with Ni−Ni separations of 5.16 and 5.12 Å, respectively. Each nickel(II) atom is placed in an octahedral NiN_6 environment: four nitrogen atoms of the amine and two nitrogen atoms of two azido bridges. The magnetic properties of the three compounds were studied by susceptibility measurements at variable temperatures (300−4 K). From the spin Hamiltonian $H = -JS_1S_2$, the calculated J value for **1** is -83.6 cm^{-1}, in good agreement with the expected value. From the spin Hamiltonian $H = -J_{1,2}(S_1S_2 + S_1S_3) - J_3(S_2S_3)$, the obtained J values are $J_{1,2} = -72(3)$ cm^{-1}, $J_3 = -36(3)$ cm^{-1} for **2** and $J_{1,2} = -60.3(3)$ cm^{-1}, $J_3 = -29.4(2)$ cm^{-1} for **3**.

Introduction

The magnetic behavior of nickel(II) dimers, in which the azide anion acts as a bidentate bridging ligand, is well-known, and the general trends of their magnetic properties are well established: generally the azido bridge propagates antiferromagnetic interactions between the two paramagnetic centers of the dinuclear compounds if the coordination mode is (1,3)[1−5] and ferromagnetic interactions if the coordination mode is (1,1).[6−10] For the dinuclear $[Ni(\mu_{1,3}\text{-}N_3)_2Ni]^{2+}$ compounds Ribas and coworkers[4] have established that the J value is strongly correlated with the dihedral angle δ, which is defined as the angle between the $(N_3)_2$ (least-squares) plane and the N(azido)−Ni−N(azido) plane. $(\mu\text{-}N_3)_2[Ni(222\text{-tet})]_2(BPh_4)_2$ (**1**) is a new complex (the fifth) which can be added to the series of dinuclear $[Ni(\mu_{1,3}\text{-}N_3)_2Ni]^{2+}$ compounds to validate the theoretical analysis.

On the other hand, the number of published trinuclear Ni(II) compounds is not very high,[11,12] and no examples have been published with azido bridging ligands. In this work, we also report the syntheses of the azido-bridged nickel(II) trinuclear compounds $(\mu\text{-}N_3)_3[Ni_3(222\text{-tet})_3](PF_6)_3$ (**2**) and $(\mu\text{-}N_3)_3[Ni_3(222\text{-tet})_3](ClO_4)_3$ (**3**) and the XANES and EXAFS spectra of compounds **1**−**3**, 1 has been used as a model, in order to obtain structural information for compounds **2** and **3**, for which it was not possible to obtain monocrystals. The data analysis reveals the occurrence of azido-bridged trinuclear nickel(II) compounds for **2** and **3** with Ni−Ni separations of 5.16 and 5.12 Å, respectively. The analysis of the magnetic susceptibility *vs* temperature data is also coherent with a triangular structure, in which two sides are equivalent to each other and different from the third.

Experimental Section

Synthesis. *Warning*! Perchlorate salts of metal complexes with organic ligands are potentially explosive. Only a small amount of material should be prepared, and it should be handled with care.

[†] Universitat de Barcelona.
[‡] Universitat de València.
[§] Technische Universität Graz.
[⊗] Abstract published in *Advance ACS Abstracts,* August 15, 1997.

(1) Wagner, F.; Mocella, M. T.; D'Aniello, M. J.; Wang, A. J. H.; Barefield, E. K. *J. Am. Chem. Soc.* **1974**, *96*, 2625.
(2) Pierpont, C. G.; Hendrickson, D. N.; Duggan, D. M.; Wagner, F.; Barefield, E. K. *Inorg. Chem.* **1975**, *14*, 604.
(3) Chauhuri, P.; Guttman, M.; Ventur, D.; Wieghart, K.; Nuber, B.; Weiss, J. J. *J. Chem. Soc., Chem. Commun.* **1985**, 1618.
(4) Ribas, J.; Monfort, M.; Díaz, C.; Bastos, C.; Solans, X. *Inorg. Chem.* **1993**, *32*, 3557.
(5) Ribas, J.; Monfort, M.; Ghosh, B. K.; Cortés, R.; Solans, X.; Font-Bardía, M. *Inorg. Chem.* **1996**, *35*, 864.
(6) Arriortua, M. I.; Cortés, A. R.; Lezama, L.; Rojo, T.; Solans, X. *Inorg. Chim. Acta* **1990**, *174*, 263.
(7) Escuer, A.; Vicente, R.; Ribas, J. *J. Magn. Magn. Mater.* **1992**, *110*, 181.
(8) Vicente, R.; Escuer, A.; Ribas, J.; El Fallah, M. S.; Solans, X.; Font-Bardia, M. *Inorg. Chem.* **1993**, *32*, 1920 and references therein.
(9) Cortés, R.; Ruiz de Larramendi, J. I.; Lezama, L.; Rojo, T.; Urtiaga, K.; Arriortua, M. I. *J. Chem. Soc., Dalton Trans.* **1992**, 2723.
(10) Ribas, J.; Monfort, M.; Díaz, C.; Bastos, C.; Solans, X. *Inorg. Chem.* **1994**, *33*, 484.
(11) Escuer, A.; Vicente, R.; Kumar, S. B.; Solans, X.; Font-Bardiá, M.; Caneschi, A. *Inorg. Chem.* **1996**, *35*, 3094.
(12) Fabretti, A. C.; Giusti, A.; Albano, V. G.; Castellari, C.; Gatteschi, D.; Sessoli, R. *J. Chem. Soc., Dalton Trans.* **1991**, 2133 and references therein.

S0020-1669(97)00247-4 CCC: $14.00

Table 1. Crystallographic Data for $(\mu\text{-}N_3)_2[Ni_2(222\text{-tet})]_2(BPh_4)_2$

empirical formula	$C_{60}H_{76}B_2N_{14}Ni_2$	Z	2
fw	1132.36	T, C	25
space group	$P2_1/n$	λ(Mo Kα), Å	0.710 69
a, Å	10.639(4)	d_{calc}, g·cm^{-3}	1.326
b, Å	19.770(7)	μ(Mo Kα), cm^{-1}	7.2
c, Å	13.609(6)	R^a	0.041
β, deg	97.78(3)	$R_w{}^b$	0.040
V, Å^3	2836(2)		

^{a} $R = \sum||F_o| - k|F_c||/\sum|F_o|$. ^{b} $R_w = [\sum w(|F_o| - k|F_c|)^2/\sum w|F_o|^2]^{1/2}$.

$(\mu\text{-}N_3)_2[Ni(222\text{-tet})]_2(BPh_4)_2$ (**1**) was synthesized by the addition of a concentrated aqueous solution of sodium tetraphenylborate (5 mmol) to 30 mL of an aqueous solution obtained by mixing 5 mmol of nickel nitrate hexahydrate, 5 mmol of triethylenetetramine (222-tet), and 5 mmol of sodium azide. The blue compound **1** precipitated immediately as a powder. **1** is slighly soluble in acetonitrile. By slight evaporation of this solvent, blue crystals of **1** suitable for X-ray determination were obtained.

$(\mu\text{-}N_3)_3[Ni_3(222\text{-tet})_3](PF_6)_3$ (**2**) was synthesized from an aqueous solution containing sodium hexafluorophosphate (5 mmol), nickel nitrate hexahydrate (5 mmol), triethylenetetramine (5 mmol), and sodium azide (5 mmol). A small quantity of nickel hydroxide was removed by filtration, and **2** was obtained as a blue crystalline powder by slow evaporation of the filtrate.

$(\mu\text{-}N_3)_3[Ni_3(222\text{-tet})_3](ClO_4)_3$ (**3**) was synthesized from an aqueous solution containing nickel perchlorate hexahydrate (5 mmol), triethylenetetramine (5 mmol), and sodium azide (5 mmol). A small quantity of nickel hydroxide was removed by filtration, and **3** was obtained as a blue crystalline powder by slow evaporation of the filtrate.

All attempts to obtain crystals suitable for X-ray determination from dilute solutions of **2** or **3** were unsuccessful. Anal. Calcd (found) for **1** ($C_{60}H_{76}B_2N_{14}Ni_2$): C, 63.7 (64.0); H, 6.8 (6.5); N, 17.7 (16.9). Calcd (found) for **2** ($C_{18}H_{54}F_{18}P_3N_{21}Ni_3$): C, 18.4 (18.9); H, 4.6 (4.7); N, 25.0 (23.9). Calcd (found) for **3** ($C_{18}H_{54}Cl_3N_{21}Ni_3O_{12}$): C, 20.8 (21.2); H, 5.2 (5.3); N, 28.3 (26.5).

Spectral and Magnetic Measurements. IR spectra were recorded from KBr pellets on a Nicolet 520 FTIR spectrophotometer. Electronic spectra were obtained on a Shimadzu UV 160 A spectrophotometer, in the 1100−200 nm range. Magnetic measurements for **1** were carried out on a polycrystalline sample with a pendulum type magnetometer (Manics DSM8) equipped with a helium continuous-flow cryostat, working in the 4.2−300 K range, and a Drusch EAF 16UE electromagnet. Magnetic measurements for **2** and **3** were carried out on polycrystalline samples using a Quantum Design SQUID susceptometer. Diamagnetic corrections were estimated from Pascal's tables.

Crystallographic Data Collection and Refinement of the Structure of $(\mu\text{-}N_3)_2[Ni(222\text{-tet})]_2(BPh_4)_2$. A transparent blue prismatic crystal (approximate size: 0.45 × 0.35 × 0.25 mm) was selected and mounted on a modified STOE four-circle diffractometer. The crystallographic data, conditions retained for the intensity data collections, and some features of the structure refinement are given in Table 1. The accurate unit-cell parameters were determined from automatic centering of 30 reflections ($9° < \theta < 16°$) and refined by least-squares methods. Intensities were collected with graphite-monochromatized Mo Kα radiation, using the ω-scan technique. A total of 6694 reflections were collected in the range $5° < 2\theta < 56°$ ($\pm h, +k, +l$), and 3182 reflections were assumed as observed by applying the conditions $F > 3\sigma(F_o)$. Two reflections ($10\bar{3}$, $03\bar{2}$) were collected every 1 h as orientation and intensity controls; significant intensity decay was not observed. Corrections were made for Lorentz−polarization effects and for absorption using the DIFABS computer program.[13] The structure was solved by a Patterson synthesis using the SHELXS computer program[14] and refined by blocked-matrix least-squares methods, using the SHELX76 computer program.[15] The function minimized was $0.9124/[\sum w(|F_o| - |F_o|)^2]$ where $w = [\sigma^2(F_o) + k|F_o|^2]^{-1}$, $k = 0.0$. f, f', and f'' were taken from ref 16. The locations of hydrogen atoms bonded to carbon atoms were computed; hydrogen atoms bonded to nitrogen atoms were located from a difference synthesis and refined with fixed N−H bond lengths. Each hydrogen atom was assigned an individual isotropic temperature factor. The final R factor was 0.041 (R_w = 0.040) for all observed reflections. The number of parameters refined was 408. Maximum shift/esd = 0.3. Maximum and minimum peaks in the final difference synthesis were 0.22 and −0.30 e Å^{-3}, respectively. Final atomic coordinates are given in Table 2.

Table 2. Relative Atomic Coordinates ($\times 10^4$) and Equivalent Isotropic Thermal Parameters (Å^2 × 10^3) for $(\mu\text{-}N_3)_2[Ni(222\text{-tet})]_2[B(Ph)_4]_2$ (**1**)

atom	x/a	y/b	z/c	$U_{eq}{}^a$
Ni	994.7(4)	876.0(2)	1339.6(4)	36.6(1)
N(1)	−478(3)	918(2)	144(2)	51(2)
N(2)	−1028(3)	478(2)	−308(2)	40(2)
N(3)	1628(3)	−65(2)	776(3)	55(2)
N(4)	90(3)	359(2)	2374(3)	47(2)
C(1)	868(4)	444(2)	3348(3)	56(3)
C(2)	2252(4)	369(2)	3191(3)	60(3)
N(5)	2514(3)	876(2)	2482(2)	44(2)
C(3)	3644(3)	820(2)	2006(3)	57(3)
C(4)	3610(3)	1360(2)	1226(3)	54(3)
N(6)	2332(3)	1417(2)	636(2)	42(2)
C(5)	1847(4)	2115(2)	507(3)	50(2)
C(6)	1337(3)	2349(2)	1429(3)	47(2)
N(7)	383(3)	1856(2)	1669(3)	43(2)
B(1)	2981(4)	1050(2)	7106(3)	35(2)
C(7)	1456(3)	1230(2)	6985(3)	36(2)
C(8)	831(3)	1374(2)	7794(3)	45(2)
C(9)	−481(4)	1457(2)	7708(4)	59(3)
C(10)	−1208(4)	1396(2)	6805(4)	64(3)
C(11)	−642(4)	1250(2)	5996(4)	62(3)
C(12)	678(3)	1167(2)	6080(3)	47(2)
C(13)	3041(3)	250(2)	7413(3)	37(2)
C(14)	3235(3)	32(2)	8401(3)	45(2)
C(15)	3191(3)	−647(2)	8666(4)	56(3)
C(16)	2948(4)	−1135(2)	7944(4)	60(3)
C(17)	2747(3)	−946(2)	6967(4)	55(3)
C(18)	2784(3)	−268(2)	6721(3)	43(2)
C(19)	3582(3)	1210(2)	6092(3)	36(2)
C(20)	4546(3)	828(2)	5758(3)	48(2)
C(21)	5125(4)	1021(2)	4950(3)	57(3)
C(22)	4772(4)	1607(2)	4442(3)	61(3)
C(23)	3828(4)	2006(2)	4746(3)	56(3)
C(24)	3264(3)	1809(2)	5566(3)	43(2)
C(25)	3846(3)	1508(2)	7931(3)	37(2)
C(26)	3503(4)	2145(2)	8247(3)	46(2)
C(27)	4327(4)	2545(2)	8870(3)	61(3)
C(28)	5543(5)	2331(3)	9197(3)	67(3)
C(29)	5926(4)	1705(3)	8900(3)	65(3)
C(30)	5092(3)	1308(2)	8277(3)	52(3)

^{a} U_{eq} is defined as one-third of the trace of the orthogonalized $\mathbf{U}_{ij}$ tensor.

X-ray Absorption Data Collection and Processing. The XANES (X-ray absorption near-edge structure) and EXAFS (extended X-ray absorption fine structure) data were collected

(13) Walker, N.; Stuart, D. *Acta Crystallogr.* **1983**, *A39*, 158.
(14) Sheldrick, G. M. *Acta Crystallogr.* **1990**, *A46*, 467.
(15) Sheldrick, G. M. SHELX: A computer program for crystal structure determination. University of Cambridge, England, 1976.
(16) *International Tables for X-ray Crystallography*; Kynoch Press: Birmingham, England, 1974; Vol. IV, pp 99−110, 149.

at LURE (Laboratoire d'Utilisation du Rayonnement Electromagnétique, Paris-Sud University) on the storage ring DCI (Dispositif des Collisitions dans l'Igloo) with an energy of 1.85 GeV and a mean intensity of 300−200 mA. The measurements were carried out at the nickel K-edge in the transmission mode on the EXAFS III spectrometer equipped with a two-crystal monochromator (Si 311, 0.5 mm entrance slit for both XANES and EXAFS). The monochromator was slightly detuned to ensure harmonics rejection. Reduced-pressure, air-filled ionization chambers were used to measure the flux intensity before and after the sample. The spectra were recorded at 10 K in a helium cryostat designed for X-ray absorption spectroscopy.

The XANES spectra were recorded step by step, every 0.25 eV with a 2 s accumulation time per point. The spectrum of a 5 μm nickel foil was recorded just after or before each XANES spectrum to check the energy calibration, thus ensuring an energy accuracy of 0.25 eV. The EXAFS spectra were recorded in the same way over 1200 eV, with 2 eV steps and a 1 s accumulation time per point. The experiments were calibrated by using the 8991.1 eV peak at the top of the edge of a metallic foil of copper and verifying that the first inflection point in all of the spectra of the nickel foils was 8332.8 eV. Each spectrum is the sum of several independent recordings added after individual inspections (two for XANES, eight (**1**) or four (**2**−**3**) for EXAFS). Samples were well-pounded microcrystalline powders of homogeneous thickness and calculated weight that were compressed between two X-ray-transparent windows. The thickness was computed in order to obtain an absorption jump at the edge of $\Delta\mu x \approx 1$ with a total absorption above the edge of less than $\Delta\mu x \approx 1.5$.

The XANES and standard EXAFS data analyses used with the GALAAD[17] and EXAFS pour le MAC[18] programs were carried out by following a well-known procedure described elsewhere.[19−21] Modeling of the outer shells was not possible in the frame of the single-scattering (SS) model; therefore, the multiple-scattering/spherical-waves EXAFS *ab initio* modeling FEFF[22−24] program was used. Multiple-scattering (MS) EXAFS contributions were included using methodology described elsewhere.[25] The FEFF calculations were performed on a RISC system/6000 running the AIX 3.2.5 program of the Physical Chemistry Department of the University of Valencia.

Results and Discussion

IR and Electronic Spectra. The IR spectra of the three compounds are similar, showing the bands attributable to the tetraamines and the anion groups (tetraphenylborate, hexafluorophosphate, and perchlorate) at normal frequencies. No bands attributable to coordinated water are observed for **1**−**3**. In the 2000−2100 cm^{-1} region, **1**−**3** present strong bands attributable to the azido ligand at 2092 (s), 2036 (shoulder, w) for **1**, 2093 (s), 2065 (m), 2027 (m) for **2**, and 2076 (s), 2047 (shoulder, m), 2027 (m) for **3**. The electronic spectra recorded with water as the solvent show the three characteristic absorptions of nickel(II) at 886, 559, 349 nm for **1**, 889, 550, 347 nm for **2**, and 920, 579, 358 nm for **3**.

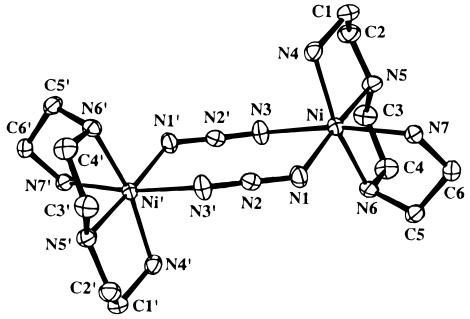

Figure 1. ORTEP drawing of the dimeric cation $(\mu\text{-}N_3)_2[Ni(222\text{-tet})]_2^{2+}$ with the atom-labeling scheme. Thermal ellipsoids are at the 50% probability level.

Table 3. Selected Bond Lengths (Å) and Angles (deg) for $(\mu\text{-}N_3)_2[Ni_2(222\text{-tet})]_2(BPh_4)_2$ (**1**)

Ni−N(1)	2.103(3)	Ni−N(3)	2.155(4)
Ni−N(4)	2.078(4)	Ni−N(5)	2.085(3)
Ni−N(6)	2.110(3)	Ni−N(7)	2.111(3)
N(1)−N(2)	1.175(5)	N(2)−N(3′)	1.169(5)
N(4)−C(1)	1.474(5)	N(5)−C(2)	1.444(6)
N(5)−C(3)	1.444(5)	N(6)−C(4)	1.486(5)
N(6)−C(5)	1.477(5)	N(7)−C(6)	1.476(5)
C(1)−C(2)	1.524(6)	C(3)−C(4)	1.503(6)
C(5)−C(6)	1.505(6)	Ni..Ni′	5.261(3)
N(1)−Ni−N(3)	89.7(1)	N(1)−Ni−N(4)	100.3(1)
N(1)−Ni−N(5)	176.6(2)	N(1)−Ni−N(6)	96.1(1)
N(1)−Ni−N(7)	84.8(1)	N(3)−Ni−N(4)	90.7(1)
N(3)−Ni−N(5)	91.0(1)	N(3)−Ni−N(6)	90.8(1)
N(3)−Ni−N(7)	171.1(1)	N(4)−Ni−N(5)	83.0(1)
N(4)−Ni−N(6)	163.5(1)	N(4)−Ni−N(7)	97.1(1)
N(5)−Ni−N(6)	80.6(1)	N(5)−Ni−N(7)	94.2(1)
N(6)−Ni−N(7)	83.0(1)	Ni−N(1)−N(2)	129.9(3)
N(1)−N(2)−N(3′)	176.3(4)	Ni−N(3)−N(2′)	128.5(3)
Ni−N(4)−C(1)	107.3(2)	Ni−N(5)−C(2)	107.3(2)
Ni−N(5)−C(3)	105.9(2)	C(2)−N(5)−C(3)	119.6(3)
Ni−N(6)−C(4)	109.9(2)	Ni−N(6)−C(5)	106.3(2)
C(4)−N(6)−C(5)	114.5(3)	Ni−N(7)−C(6)	108.5(2)
N(4)−C(1)−C(2)	107.3(3)	N(5)−C(2)−C(1)	107.7(3)
N(5)−C(3)−C(4)	108.7(3)	N(6)−C(4)−C(3)	111.6(3)
N(6)−C(5)−C(6)	110.4(3)	N(7)−C(6)−C(5)	108.6(3)

Description of the Structure of 1. A view of a dinuclear unit with the atom-labeling scheme is shown in Figure 1, and selected bond lengths and angles are given in Table 3. The structure consists of independent dinuclear $(\mu\text{-}N_3)_2[Ni(222\text{-tet})]_2^{2+}$ cations and two tetraphenylborate anions. The nickel atom is placed in a distorted octahedral environment formed by the four N atoms of the tetraamine and the two terminal N atoms of the bridging azido ligands. The six bond distances around the nickel atom are very close, ranging from Ni−N(4) = 2.085(3) Å to Ni−N(3) = 2.155(4) Å. The central $Ni(N_3)_2$-Ni core has an inversion center with Ni−N(azido) distances of 2.103(3) and 2.155(4) Å for Ni−N(1) and Ni−N(3), respectively. The six N(azido) atoms of the central $Ni(N_3)_2Ni$ core are in the same plane (no deviations from the mean plane). The N−Ni−N angles are 89.7°, and the Ni−N(1)−N(2) and Ni−N(3)−N(2′) angles are 129.9(3) and 128.5(3)°, respectively. The dihedral angle δ, which is defined as the angle between the $(N_3)_2$ plane and the N(azido)−Ni−N(azido) plane[4] is 22.4(2)°, giving a chairlike structure.

Structural Characterization of 2 and 3. The absence of single crystals of **2** and **3**, and their poor crystallinity, prevented

(17) Noinville, V.; Michalowicz, A. *GALAAD*; Société Française de Chimie: Paris, 1991; pp 116−117.
(18) Michalowicz, M. *EXAFS pour le MAC*; Société Française de Chimie: Paris, 1991; pp 102−103.
(19) Teo, B. K. *EXAFS: Basic principles and data analysis*; Springer-Verlag: Berlin, 1986; Vol. 9.
(20) Königsberger, D. C.; Prins, R. *X-Ray Absorption Principles, and Applications, Techniques of EXAFS, SEXAFS, and XANES*; John Wiley: New York, 1988.
(21) Lytle, F. W.; Sayers, D. E.; Stern, E. A. *Physica* **1989**, *B158*, 701.
(22) Rehr, J. J. *Jpn. J. Appl. Phys*. **1993**, *32*, 8.
(23) Rehr, J. J.; Zabinsky, S. I.; Albers, R. C. *Phys. Rev. Lett*. **1992**, *69*, 3397.
(24) Rehr, J. J.; Mustre de Léon, J.; Zabinsky, S. I.; Albers, R. C. *J. Am. Chem. Soc*. **1991**, *113*, 5135.
(25) Michalowicz, A.; Moscovici, J.; Ducourant, B.; Cracco, D.; Kahn, O. *Chem. Mater*. **1995**, *7*, 1833−1842.

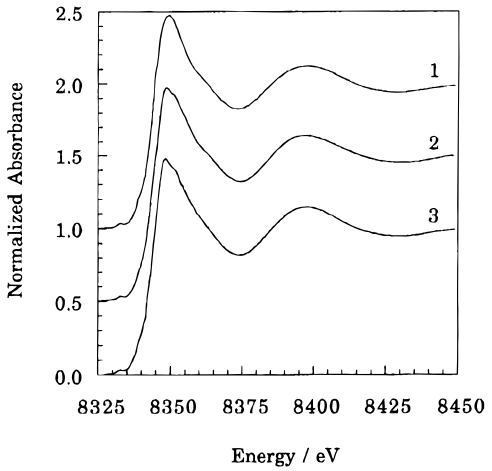

Figure 2. Normalized XANES spectra at the nickel K-edge for **1**−**3** at 10 K.

us from obtaining structural information by the common X-ray diffraction techniques. Therefore, we decided to study the XANES and EXAFS spectra of **2** and **3**, with **1** as model. The use of X-ray absorption techniques in this structural area is not new, and they have been previously revealed as very useful tools in coordination chemistry.[25−30]

The normalized XANES spectra of compounds **1**−**3** at the nickel K-edge are given in Figure 2. Two facts emerge from this figure: (i) The three spectra are almost superimposable as to their shapes and transition energies, suggesting strong similarities in the geometries around the metal ions. The change in nuclearity does not greatly disturb the nickel coordination sphere. (ii) The edges are typical of octahedral Ni(II) complexes with a 1s ↔ 3d pre-edge feature at 8332.7 eV and an absorption edge centered on ∼8349 eV. The intensity of the pre-edge is weak, which indicates that Ni(II) is located on a (quasi) inversion center, where such transitions are symmetry forbidden.[31]

The top of the edge of **1** is featureless, showing that the deformation of the octahedral environment is weak.[32] However, for compounds **2** and **3**, a weak structure can be seen at the top of the edge, a little more significant for the latter. Two interpretations are possible: either a transition to bound states or an intermediate-scattering scheme.[33,34] The observed evolutions would be assigned to a splitting of the t_{1u}* metal orbitals in the frame of the former interpretation and to slightly different multiple-scattering pathways in the frame of the latter. The two views, however, converge to the same conclusion: a distortion of the octahedral environment in compounds **2** and **3** with respect to **1**.[35]

The *k*-space experimental EXAFS spectra $k\chi(k)$ *vs* k at 10 K for **1**−**3**, at the nickel K-edge, and the corresponding Fourier transforms are given in Figure 3. Absorption data were collected to $k = 15$ Å^{-1}, resulting in good resolution of peaks in the Fourier transforms. The similarity of the experimental $k\chi(k)$ values and their Fourier transforms corresponding to the dinuclear model compound and complexes **2** and **3** allows us to assume that the local structure of the Ni(II) ion is almost the same for the three compounds, the slight differences being attributed to the presence of two nickel neighbors in compounds **2** and **3** instead of only one in the dinuclear model complex. In particular, the amplitudes of the EXAFS oscillations appear unchanged. Then, there is the same number of nearest neighbors in the three compounds. Fourier transforms for **1**−**3** comprise two main peaks: the first one corresponds to six nitrogen atoms, four from the amine ligand and two from the nearest nitrogens of the azide bridges, and the second one corresponds to the carbon atoms belonging to the same amine ligand and the two second nitrogen atoms from the azide bridges. It is particularly important to examine the Fourier transforms of these two main peaks: an additional weak signal is present at a distance of ∼5 Å, which is tentatively assigned to the intramolecular nickel−nickel distance as the major contribution (see discussion below). The middle zone corresponds to the two third nitrogen atoms of the azide bridges.

Within the frame of the single-scattering approach, we analyzed the first coordination sphere: the Ni(II) ion is surrounded by six nitrogen atoms with average Ni−N bond distances of 2.11 Å for complexes **1** and **2** and 2.10 Å in the case of **3**. However, a complete quantitative assessment of the local structure around the metal ions including atoms in a sphere of 6 Å cannot be performed correctly in the frame of the single-scattering approach of the standard EXAFS formula.[36] In fact, as illustrated in Chart 1 for complex **1**, it can be seen that, beyond the single backscattering paths (nleg = 2, nleg being the number of scattering segments in the FEFF program), several paths with nleg = 3 (a and b), 4 (c), and 5 (d) are present. They are also significant and cannot be neglected. That being so, we have performed an FEFF calculation using **1** as a model compound for the environment of the nickel ion in **2** and **3**. Since the peak around 5 Å will provide important information on the structure, we verified that this peak was not due to an artifact: (i) the background was carefully analyzed by Fourier transform in order to ensure that there was no spurious signal around 5 Å in the background of the spectrum; (ii) it can be seen from the Fourier transform (Figure 3) that this peak is above the noise level; (iii) accidental fluctuations in X-ray intensity were observed in neither the incoming I_0 nor the transmitted beam I; and (iv) the quality and homogeneity of the sample were carefully checked. As a matter of fact, the comparison of the FEFF calculation and the spectrum resulting from the same model but without heavy neighbors (Figure S1, Supplementary Information) shows that there is a peak around 5 Å in the former but not in the latter. Therefore, we can say that the 5 Å signal is not due to an experimental or mathematical artifact but arises from heavy neighbors. The quality of the FEFF model compared to the experimental spectrum is illustrated in Figure 4a. The $k\chi(k)$ data and the imaginary part of the radial distribution function for compound **1** are compared to the theoretical model including 103 scattering paths, calcu-

(26) Lloret, F.; Ruiz, R.; Julve, M.; Faus, J.; Journaux, Y.; Castro, I.; Verdaguer, M. *Chem. Mater.* **1992**, *4*, 1150.
(27) Gadet, V.; Mallah, T.; Castro, I.; Verdaguer, M. *J. Am. Chem. Soc.* **1992**, *114*, 9213.
(28) Lloret, F.; Ruiz, R.; Cervera, B.; Castro, I.; Julve, M.; Faus, J.; Real, J. A.; Sapiña, F.; Journaux, Y.; Colin, J. C.; Verdaguer, M. *J. Chem. Soc., Chem. Commun.* **1994**, 2615.
(29) Ruiz, R.; Surville-Barland, C.; Journaux, Y.; Colin, J. C.; Castro, I.; Cervera, B.; Julve, M.; Lloret, F.; Sapiña, F. *Chem. Mat.* **1996**, in press.
(30) Real, J. A.; Castro, I.; Buosseksou, A.; Verdaguer, M.; Burriel, R.; Linares, J.; Varret, F. *Inorg. Chem.*, in press.
(31) Roe, A. L.; Schneider, D. J.; Mayer, R. J.; Pyrz, J. W.; Widom, J.; Que, L., Jr. *J. Am. Chem. Soc.* **1984**, *106*, 1676.
(32) Rakotonandasana, A.; Boinnard, D.; Savariault, J.-M.; Tuchages, J.-P.; Petrouleas, V.; Cartier, C.; Verdaguer, M. *Inorg. Chim. Acta* **1991**, *180*, 19.
(33) Natoli, C. R.; Benfatto, M.; Doniach, S. *Phys. Rev. A* **1986**, *34*, 4682.
(34) Benfatto, M.; Natoli, C. R.; García, J.; Bianconi, A.; Marcelli, A.; Fanfoni, M.; Davoli, I. *Phys. Rev. B* **1986**, *34*, 5774.
(35) Nakatani, K.; Carriat, J. Y.; Journaux, Y.; Kahn, O.; Lloret, F.; Renard, J. P.; Pei, Y.; Sletten, J.; Verdaguer, M. *J. Am. Chem. Soc.* **1989**, *111*, 5739.
(36) Zhang, H. H.; Filipponi, A.; Cicco, A. D.; Lee, S. C.; Scott, M. J.; Holm, R. H.; Hedman, B.; Hodgson, K. O. *Inorg. Chem.* **1996**, *35*, 4819−4828.

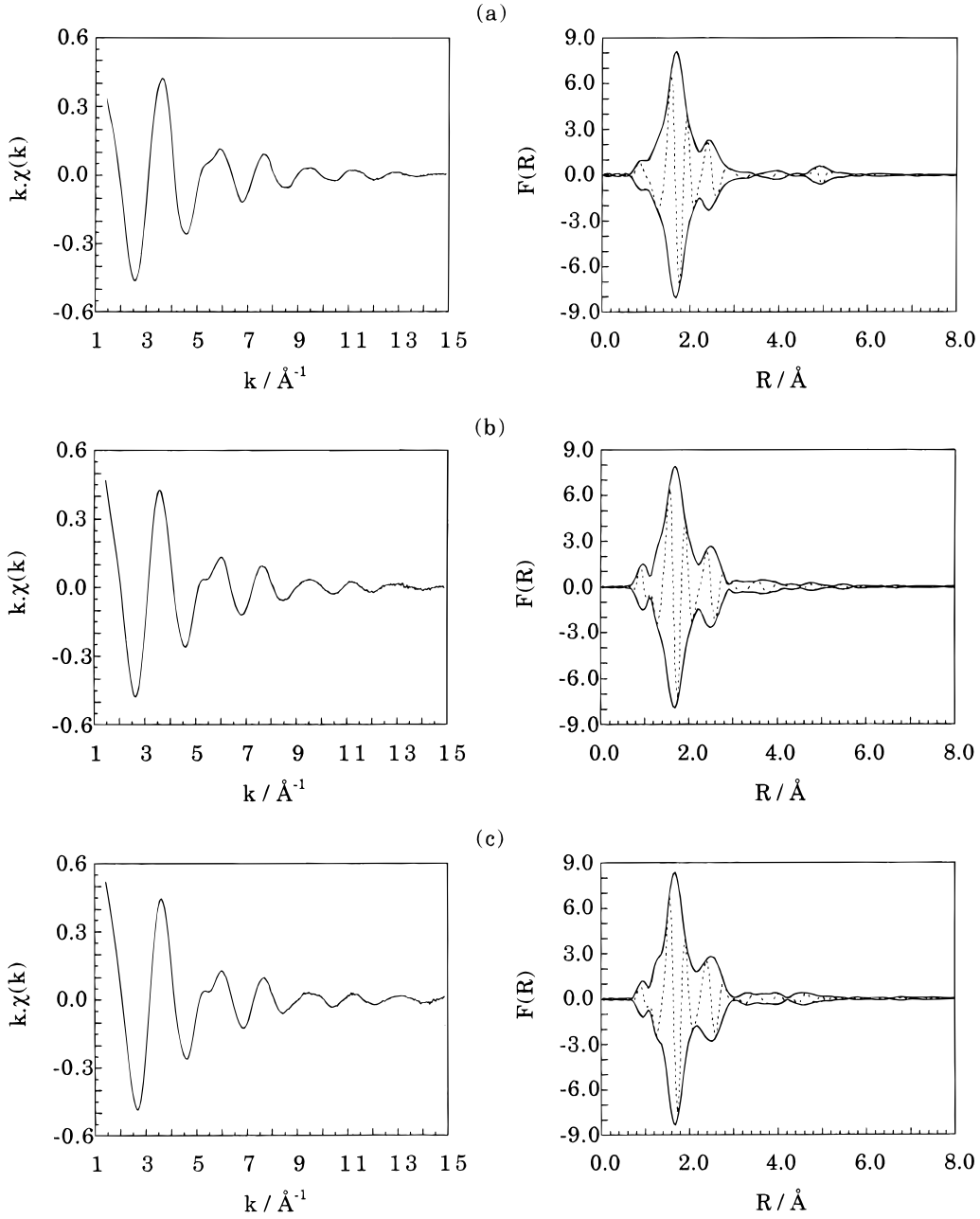

Figure 3. *k*-space experimental EXAFS spectra $k\chi$(k) *vs k* (left) and their Fourier transforms of the EXAFS spectra (right) at the nickel K-edge for **1** (a), **2** (b), and **3** (c) at 10 K.

Chart 1

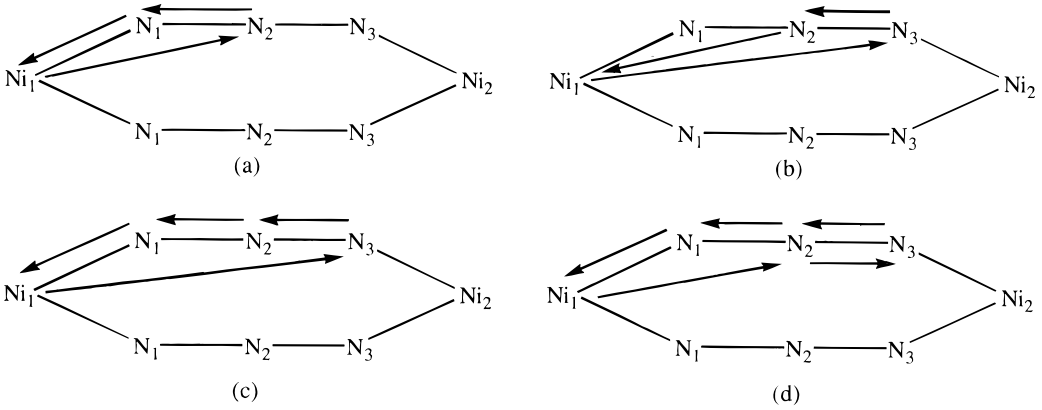

lated by FEFF on the complete set of atomic coordinates of **1**. The large number of pathways determined by FEFF is due to the fact that the symmetry of the model compound is low and thus the degeneracy is weak. Using the dinuclear complex as

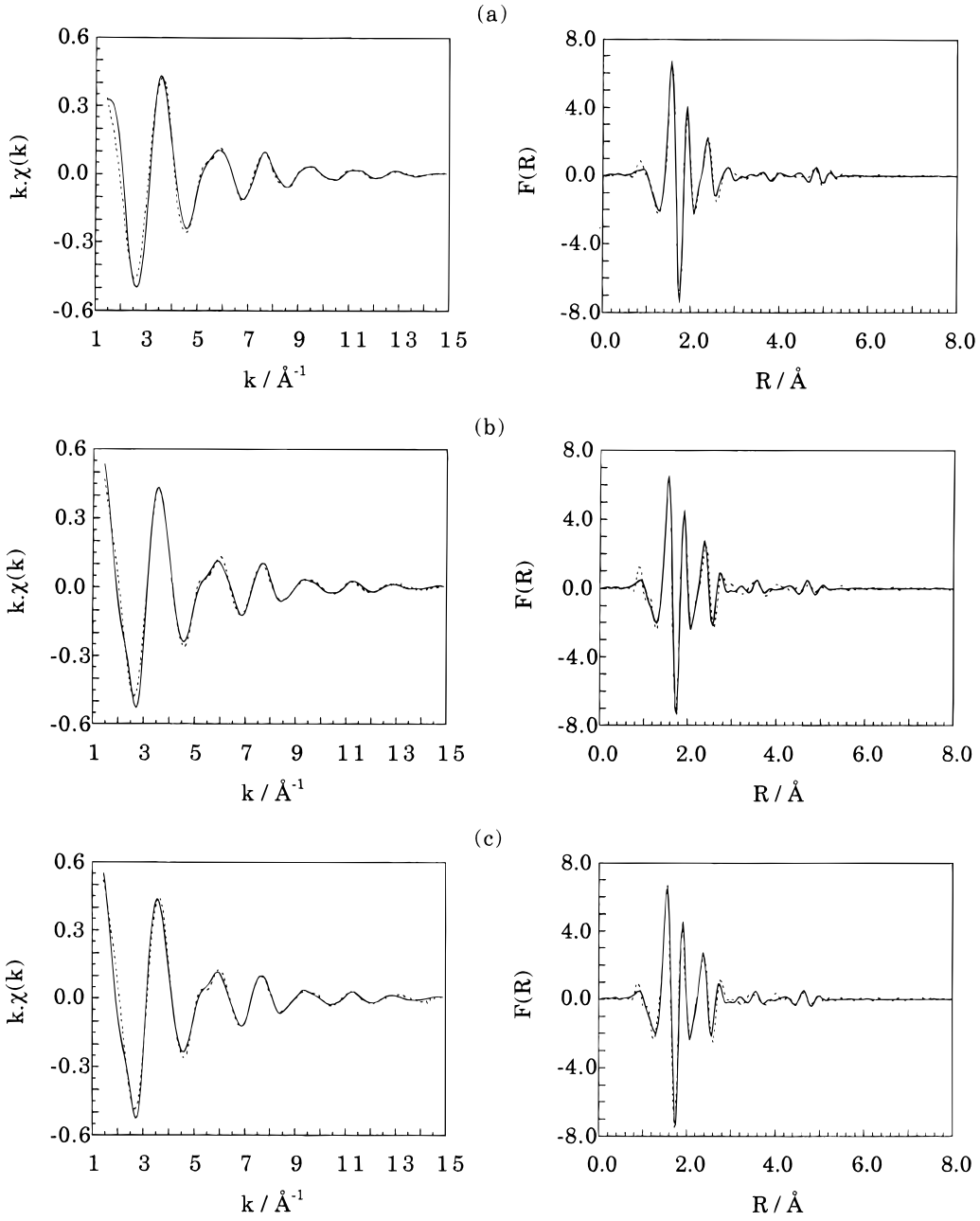

Figure 4. Comparison of the experimental (dashed lines) and calculated spectra (solid lines) using the FEFF method on the dinuclear model compound for **1** (a) and the postulated trinuclear compound for **2** (b) and **3** (c): $k\chi(k)$ values (left); imaginary parts of the Fourier transforms (right).

the starting structure, we built a schematic trinuclear model for compounds **2** and **3**:

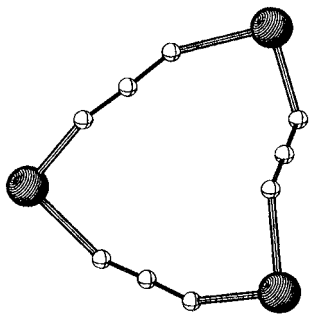

Parts b and c of Figure 4 show the comparisons between experimental data and the theoretical trinuclear model. The spectra compare quite well in both phase and amplitude, especially at short and long distances.

We also analyzed quantitatively the first and outer shells of compounds **1**−**3** by using the amplitudes and phase shifts extracted from the FEFF calculations, including the most important multiple-scattering pathways ((a) and (b) in Chart 1). The number and postulated nature of neighbors, the absorber−neighbor distances, the Debye−Waller factors, and other parameters resulting from quantitative MM analyses of the EXAFS data are available in Table 4. These data confirm the above qualitative discussion. The resulting average distances for compounds **1**−**3** are the following: six nitrogen atoms at 2.11, 2.11, and 2.10 Å, respectively (the same distances as found by simple-scattering analysis, as expected), six carbon atoms at 2.90, 2.95, and 2.95 Å, two nitrogen atoms at 3.01, 3.06, and 3.03 Å, two nitrogen atoms at 4.05, 4.11, and 4.13 Å, and, finally, one nickel atom at 5.27 for **1** and two metal ions at 5.16 and 5.12 Å for **2** and **3**, respectively. These distances compare well with the crystallographic average distances in **1**. Least-squares refinement resulted in the simulation shown in

Table 4. Fitting of the EXAFS Data for Compounds **1**−**3**[a−c]

	1[d]	**2**	**3**
	First Shell		
N_1	6 N	6 N	6 N
R_1,Å	2.11(1)[e]	2.11(1)	2.10(2)
s_1,Å	0.00	0.00	0.00
	Second Shell		
N_2	6 C	6 C	6 C
R_2,Å	2.90(3)	2.95(4)	2.95(3)
s_2,Å	0.07	0.06	0.06
	Third Shell		
N_3	2 N	2 N	2 N
R_3,Å	3.01(2)	3.06(2)	3.03(3)
s_3,Å	0.11	0.10	0.10
	Fourth Shell		
N_4	2 N	2 N	2 N
R_4,Å	4.05(2)	4.11(3)	4.13(3)
s_4,Å	0.12	0.12	0.13
	Fifth Shell		
N_5	1 Ni	2 Ni	2 Ni
R_5,Å	5.27(1)	5.16(5)	5.12(2)
s_5,Å	0.08	0.12	0.11
G	0.7	0.7	0.8
ρ,%	0.6	1.3	1.9

[a] The fit was performed by including the amplitude and phases extracted from the FEFF calculation. [b] The results of the SS fit of the first shell using the theoretical amplitudes and phases of McKale[40] are 2.11, 2.11, and 2.10 Å for compounds **1**−**3**, respectively, for the Cu−N distances. [c] N represents the number of atoms at the distance R from the nickel absorber, s is the Debye−Waller coefficient, G relates to the mean-free path of the electron, and ρ is the least-squares fitting parameter defined as $\rho(\%) = \Sigma[k\chi_{exp}(k) - k\chi_{th}(k)]^2/\Sigma[k\chi_{exp}(k)]^2$. [d] The average crystallographic distances for complex **1** are 2.106, 2.90, 3.01, 4.07, and 5.26 Å. [e] Errors are given in parentheses.

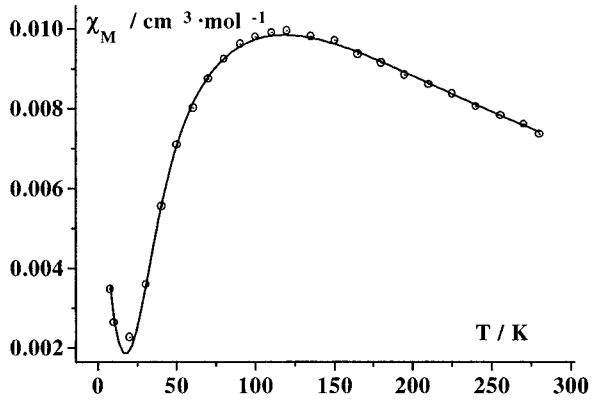

Figure 5. Thermal variation in the molar susceptibility for complex **1**. The solid line corresponds to the best theoretical fit (see text).

Figure S2, Supplementary Information. This gives an excellent fit except around $k = 3-4.5$ Å^{-1}, where the multiple scattering is more important.

Magnetic Properties. The χ_M *vs* T plot for compound **1** is shown in Figure 5. Starting from room temperature ($\chi_M = 7.37 \times 10^{-3}$ cm^3·mol^{-1}), the χ_M value increases, reaching a maximum of 9.94×10^{-3} cm^3·mol^{-1} at 120 K, and then decreases, reaching a minimum at 20 K. The next increase in the χ_M values is indicative of the presence of a small quantity of paramagnetic impurities. From the isotropic spin Hamiltonian $H = -JS_AS_B$, where J is the exchange integral and $S_A = S_B = 1$, the expression of χ_M is[37]

$$\chi_M = (2N\beta^2g^2/kT)(\exp(\alpha) + \exp(3\alpha))/(1 + 3\exp(\alpha) + 5\exp(3\alpha))$$

in which $\alpha = J/kT$ and N, β, k, and g have their usual meanings.

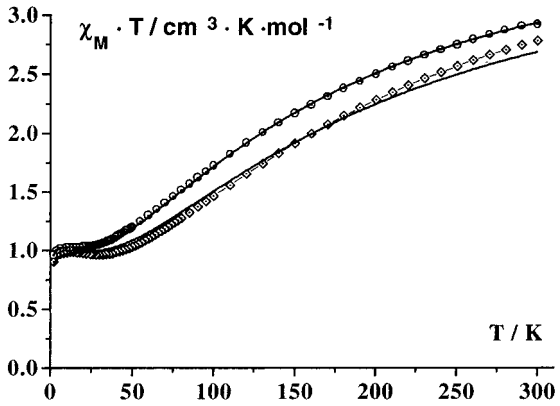

Figure 6. Thermal variation in the molar susceptibility for complexes **2** (◇) and **3** (○). The solid lines correspond to the best theoretical fits (see text).

Least-squares fitting of experimental magnetic data with the above equation gave the superexchange parameters $J = -83.6(4)$ cm^{-1}, $g = 2.43$, and $R = 4.2 \times 10^{-5}$ for **1**, where R is the quality factor defined as $R = \Sigma(\chi_M^{calc} - \chi_M^{obs})^2/\Sigma(\chi_M^{obs})^2$.

In a previous report on a series of dinuclear $\mu_{1,3}$-azido-bridged nickel(II) compounds, $Ni_2(N_3)_2$, Ribas and co-workers[4] demonstrated that the J value is strongly correlated with the dihedral angle δ (as defined above). The value of the superexchange parameter $J = -83.7$ cm^{-1} for **1** is in the range of the expected value. For a dihedral angle of 45°, the J value is -4.6 cm^{-1}; for $\delta = 20.7°$, the J value is -70 cm^{-1}; for $\delta = 34.6°$, the J value is -29.1 cm^{-1}; and for $\delta = 3.0°$, the J value is -114.5 cm^{-1}. In the current case, $\delta = 22.4°$ and the J value is -83.7 cm^{-1}, very similar to the J value found for a similar δ angle of 20.7° (-70 cm^{-1}).

Plots of the χ_MT product plotted *vs* temperature for compounds **2** and **3** are shown in Figure 6. The plots are characteristic of a strongly coupled trimer with local $S = 1$. Starting from room temperature, the χ_MT value decreases, reaching the value of 1 cm^3·K·mol^{-1} at 4 K. From the analytical and structural data we can suppose a triangular structure:

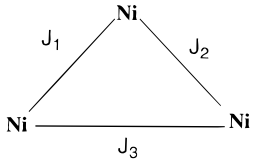

Assuming $J_{1,2} \neq J_3$ and taking into account the behavior of χ_MT at low temperature, experimental data were fitted to the expression

$$\chi_MT = N\beta g^2T(f(J,T)/kT - zJ'\,f(J,T))$$

in which zJ' is the intertrimer exchange parameter and $f(J,T)$ is

$$f(J,T) = \{6 + 6\exp(E_2) + 30\exp(E_3) + 6\exp(E_4) + 30\exp(E_5) + 84\exp(E_6)\}/\{3 + \exp(E_1) + 3\exp(E_2) + 5\exp(E_3) + 3\exp(E_4) + 5\exp(E_5) + 7\exp(E_6)\}$$

In this case, the E_n values can be obtained using the Kambe method[38] from the Hamiltonian

(37) O'Connor, C. J. *Prog. Inorg. Chem.* **1982**, *29*, 239.
(38) Kambé, K. *J. Phys. Soc. Jpn.* **1950**, *5*, 48.

$$H = -J_{1,2}(S_1S_2 + S_1S_3) - J_3(S_2S_3)$$

and

$$E_1 = J_{1,2} - 2J_3 \qquad E_2 = 2J_{1,2} - 2J_3 \qquad E_3 = 2J_{1,2}$$

$$E_4 = 3J_{1,2} - 3J_3 \qquad E_5 = 4J_{1,2} - 2J_3 \qquad E_6 = 5J_1$$

The best-fit parameters obtained for **2** and **3** by minimizing the R factor $\Sigma(\chi_M T^{calc} - \chi_M T^{obs})^2/\Sigma(\chi_M T^{obs})^2$ were $J_{1,2} = -72(3)$ cm^{-1}, $J_3 = -36(3)$ cm^{-1}, $g = 2.30(2)$, $zJ' = -0.14(63)$ cm^{-1}, $R = 2.4 \times 10^{-3}$ for **2** and $J_{1,2} = -60.3$ (3) cm^{-1}, $J_3 = -29.4(2)$ cm^{-1}, $g = 2.34$, $zJ' = -0.21(1)$ cm^{-1}, $R = 6.3 \times 10^{-5}$ for **3**.

The above results are coherent with the assumption of a triangular array of nickel atoms. Therefore, the susceptibility data indicate that the triangles are not magnetically regular and almost one of the azido bridges is not equivalent to the other two. This feature is compatible with the average Ni−Ni and Ni−N distances provided for the EXAFS measurements of **2** and **3** because the magnetic behavior is strongly dependent on the variation of the Ni−N−N bond angles and of the Ni−N_1−N_2−N_3−Ni′ torsion angles.[35] Ni−N_1 is independent of the bond angles whereas even relatively important changes in the bond angles produce very slight variations in the Ni−Ni′, Ni−N_2, and Ni−N_3 distances.

Conclusions

Analytical, magnetic, and EXAFS data are in good agreement with the assumption of a distorted triangular array for the two compound (μ-N_3)$_3$[Ni_3(222-tet)$_3$](PF_6)$_3$ (**2**) and (μ-N_3)$_3$[Ni_3(222-tet)$_3$](ClO_4)$_3$ (**3**). This new topology for the azido polynuclear derivatives is also one of the scarce examples of nickel(II) triangles, which in this case show a very high $J_3/J_{1,2}$ close to the spin frustration ratio of 0.5. In addition, the dinuclear (μ-N_3)$_2$[Ni_2(222-tet)]$_2$(BPh_4)$_2$ (**1**) compound has been studied, and its magnetic properties have been correlated to the previously reported model for chair-distorted nickel−azido dimers. An EXAFS study of **1** provided a good model for assigning the triangular array to **2** and **3** despite the large Ni···Ni distance.

Acknowledgment. We wish to express our gratitude to Dr. F. Villain for his help in the use of the EXAFS 3 spectrometer and cryogen device and Prof. Michalowicz from LURE for his help in the use of the FEFF program and fruitful discussions. Financial support from the Dirección General de Investigación Científica y Técnica (DGICYT) (Spain) through Projects PB93/0772 and PB95/1002 and from LURE (France) through Project CC303 is gratefully acknowledged.

Supporting Information Available: Text giving a structure determination summary for **1**, tables of hydrogen positional coordinates and anisotropic displacement parameters, and complete bond lengths and angles for **1**, a modulus of the Fourier transforms of the FEFF calculation on the model compound **1** with and without heavy neighbors (Figure S1), and simulations of the EXAFS data and imaginary parts of the Fourier transforms for compounds **1**−**3** using the parameters extracted from the FEFF calculation (Figure S2) (16 pages). Ordering information is given on any current masthead page.

IC9702476

(39) Escuer, A.; Vicente, R.; Ribas, J.; El Fallah, M. S.; Solans, X.; Font-Bardia, M. *Inorg. Chem.* **1994**, *33*, 1842.
(40) McKale, A. G.; Veal, B. W.; Paulikas, A. P. *J. Am. Chem. Soc*. **1988**, *110*, 3763.